Carbohydrate Polymers 82 (2010) 706–713

Contents lists available at ScienceDirect

Carbohydrate Polymers

journal homepage: www.elsevier.com/locate/carbpol

Iron(II) cross-linked chitin-based gel beads: Preparation, magnetic property and adsorption of methyl orange

Guoxiang Li[a,d], Yumin Du[a,*], Yongzhen Tao[b], Hongbing Deng[a], Xiaogang Luo[c], Jianhong Yang[a]

[a] School of Resource and Environmental Science, Wuhan University, Wuhan 430079, China
[b] Key Laboratory of Green Processing and Functional Textiles of New Textile Materials, Ministry of Education, Wuhan University of Science and Engineering, Wuhan 430073, China
[c] Department of Chemistry, Wuhan University, Wuhan 430072, China
[d] School of Chemical and Environmental Engineering, Hubei University for Nationalities, Enshi 445000, China

ARTICLE INFO

Article history:
Received 25 March 2010
Received in revised form 20 May 2010
Accepted 21 May 2010
Available online 1 June 2010

Keywords:
Magnetic nanoparticles-chitin beads
Ionic cross-linking
Adsorption
Organic dyes

ABSTRACT

Chitin/alginate magnetic nano-gel beads (MCAs) were successfully prepared from 8 wt.% NaOH/4 wt.% urea aqueous solution by ionic cross-linking. Their structure and properties were investigated using scanning electron microscopy, X-ray diffraction, and vibrating sample magnetometry. The results showed that the magnetic iron oxide nanoparticles synthesized in situ with a mean diameter of 30 nm were uniformly dispersed and immobilized in the chitin/alginate matrix. The structure and nature of iron oxide were conserved perfectly, and the MCAs had extremely small hysteresis loop and low coercivity. Moreover, MCAs could efficiently adsorb the methyl orange from wastewater. The iron oxide nanoparticles in the MCAs played an important role in both the creation of the magnetic-induced transference and the improvement of the adsorption capacity. This work provides a novel, low-cost, simple, and "green" process for synthesizing the chitin-based magnetic nanocomposite gel beads, which had potential application on the removal of hazardous materials.

1. Introduction

Recently, magnetic nanoparticles are of great interest for researchers from a wide range of areas, including magnetic fluids (Morais, Santos, Silveira, & Oliveira, 2007; Oliveira, Rossi, Jardim, & Rubim, 2009), catalysis (Zheng, Duanmu, & Gao, 2006; Arai et al., 2008), biotechnology/biomedicine (Tartaj, Morales, Veintemillas-Verdaguer, Gonzalez-Carreno, & Serna, 2003; Soenen, Hodenius, & De Cuyper, 2009), magnetic resonance imaging (Wan, Cai, Meng, & Liu, 2007; Jarzyna et al., 2009), data storage (Tansil, Ramanujan, & Li, 2003; Mironov & Ermolaeva, 2009) and environmental remediation (Liu, 2006; Sun et al., 2009). In most of the envisaged applications, polysaccharides magnetic nanocomposites display a unique attraction (Gruttner, Rudershausen, & Teller, 2001; Ma, Qi, Maitani, & Nagai, 2007; Luo, Liu, Zhou, & Zhang, 2009), which has excellent biocompatibility, admirable biodegradability with ecological safety. A number of suitable methods have been developed for the synthesis of magnetic nano-materials of various different polymers (Kroll & Winnik, 1996; Liu, Zhang, Zhou, & Wu, 2008). Generally, magnetic polymer nano-materials are prepared mainly through a two-step synthetic method as follows (Liu, Zhou, Zhang, Guan, & Wang, 2006; Ge et al., 2009; Luo & Zhang, 2009): Either magnetic nanoparticles are synthesized firstly, afterwards, mixed with polymers, or the polymer materials are prepared initially, and then, as a template, magnetic nanoparticles have been synthesized in situ. However, an unavoidable problem associated with the method is their intrinsic characteristics of longer process and high energy consumption, which must be further improved. A one-step synthetic method is relatively simple, and is clearly superior to the two-step method in economy. However, polysaccharides magnetic nanocomposite beads prepared via a one-step synthetic method have been reported rarely (Kroll & Winnik, 1996; Rocher, Siauque, Cabuil, & Bee, 2008). In particular, chitin based magnetic nanocomposite material has not been reported.

Chitin and alginate are among the most versatile marine biopolymers (Shi et al., 2005). Chitin is a linear polysaccharide composed of β-(1-4)-linked 2-acetamido-2-deoxy-D-glucose units, and is insoluble in common solvents, which has limited the further utilization of this natural biopolymer to a small area (Zheng, Zhou, Du, & Zhang, 2002; Rinaudo, 2006). Alginates are a family of linear polymers, which contain varying amounts of 1,4-linked β-D-mannuronic acid and α-L-guluronic acid residues. Alginate beads prepared by gelling with Ca^{2+} have been widely investigated in oral and nasal drug release studies (Suckow, Jarvinen, HogenEsch, Park, & Bowersock, 2002; Acosta, Aranaz, Peniche, & Heras, 2003). As environmental friendly materials, both chitin and alginate have versatile biological activities. They are thus good candidates for biological materials. Chitin are difficult to be cross-linked with metal

* Corresponding author. Tel.: +86 27 6877 8501; fax: +86 27 6877 8501.
E-mail address: duyumin@whu.edu.cn (Y. Du).

0144-8617/$ – see front matter © 2010 Elsevier Ltd. All rights reserved.
doi:10.1016/j.carbpol.2010.05.040

ions, but could accumulate metal ions and organic dyes, which has potential application in dealing with wastewater containing heavy metal ions and dyes (Zhou, Zhang, & Guo, 2005; Akkaya, Uzun, & Guzel, 2009; Miretzky & Cirelli, 2009). However, when used as adsorbents, it was quite difficult to separate chitin from the water rapidly after adsorption of the impurities. Moreover, some of these impurities were very precious, and need to be recovered. So it was a great interesting work to seek new methods for the separation of the chitin from the wastewater efficiently. And the magnetic materials could be separated from the wastewater rapidly and efficiently with the aid of magnetic force since the magnetic forces were much greater than gravitation.

In this study, we focus mainly on a convenient and "green" route to synthesize magnetic nano-gel beads by ionically cross-linked chitin/alginate, which can effectively adsorbed methyl orange. In our previous work, 8 wt.% NaOH/4 wt.% urea aqueous solution precooled to −20 °C has been developed to dissolve chitin, leading to the formation of a transparent chitin solution (Hu et al., 2007). Moreover, a chitin/alginate fibres has been fabricated from chitin and alginate solution (Hu, Du, Li, & Wang, 2008), which indicated that the two polysaccharides had good miscibility. More recently, we found that alginatel/carboxyl chitin beads for oral delivery of protein drugs could be prepared from polymer solution by using the ionically cross-linked method at room temperature (Shi et al., 2005). Encouraged by these findings, we attempted to fabricate magnetic chitin/alginate beads via in situ synthesis of iron oxide nanoparticles into the chitin/alginate matrix prepared from the NaOH/urea aqueous system. Their magnetic properties and the adsorption of methyl orange were investigated to evaluate the effects of the embedding of the iron oxide nanoparticles in the chitin/alginate matrix on the structure and properties of the materials. We hope to provide a new "green" pathway for the fabrication of magnetic chitin-based beads, which has potential application on the removal of hazardous materials from wastewater.

2. Experimental

2.1. Materials

Chitin sample (Crab shell, α-chitin) was provided by Shangdong jinhu Chitin Co., Ltd, powered, and sifted to select less than 0.635 mm diameter particles. Its viscosity average molecular weight (M_η) was determined using an Ubbelohde viscometer in NaOH/urea aqueous solution at 25 ± 0.1 °C and calculated from the Mark–Houwink equation (Li et al., 2010) $[\eta] = 0.26M_w^{0.56\pm0.02}$ (mL g^{-1}) to be 2.1×10^6. The degree of acetylation (*DA*) was measured to be 0.97 according to the previous literature method (Xu, Mccarthy, Gross, & Kaplan, 1996). The methyl orange (MO) was purchased from Sinopharm Chemical Reagent Co., Ltd, and was used as received. Other analytical-grade chemical regents were purchased in China and used without further purification.

2.2. Preparation of chitin/alginate magnetic gel beads

Approximately 2 wt.% chitin solution in 8 wt.% NaOH/4 wt.% urea was prepared according the previous method (Hu et al., 2007; Li et al., 2010). About 4 g of chitin were dissolved in 200 g 8 wt.% NaOH/4 wt.% urea aqueous solution to obtain a clear chitin solution (**I**). 16 g of sodium alginate were dissolved in 800 g 8 wt.% NaOH/4 wt.% urea aqueous solution at room temperature to obtain alginate solution (**II**). The Fe^{2+}-chitin/alginate beads were prepared by dropping aqueous chitin/alginate into a iron dichloride solution. A mixture of **I** and **II** with determined chitin/alginate weight ratios was prepared with stirring and centrifuged for 20 min under 4000 rpm to remove air bubble. The solution was then dropped through a 0.45-mm diameter syringe needle at a rate of 1.5 mL min^{-1} into 0.5 M iron dichloride aqueous solution containing 3 wt.% of hydrochloric acid with gentle agitation. The pale-yellow Fe(II)-cross-linked beads, about 2 mm in diameter, formed instantaneously. At the end of the addition, the beads were kept in the reaction solvent, and were allowed to cross-link with Fe^{2+} for 30 min at room temperature, then were collected by filtration and washed with copious amounts of water to remove unreacted Fe^{2+} on the surface. After that, the Fe(II)-cross-linked beads were then transferred to another container containing an aqueous solution of sodium hydroxide (2 mol L^{-1}, 300 mL) and treated for 20 min. The treated beads were washed with deionized water and dried at ambient temperature. Composite beads with chitin/alginate weight ratios of 2:1, 1:1, and 1:2 were labeled as MCA1, MCA2, and MCA3, respectively. The beads without alkali treatment obtained from chitin/alginate weight ratios of 1:1 were coded as CA.

2.3. Characterizations and magnetic property measurement

Scanning electron microscopy (SEM) was performed on a FESEM (SEM, SIRION TMP, FEI) using an accelerating voltage of 20 kV. The beads in the wet state were frozen in liquid nitrogen and freeze-dried using a lyophilizer (CHRIST Alpha 1–2, Germany). The freeze-dried beads were coated with Pt for the SEM observation. The samples were ground into powder and dried in a vacuum oven at 60 °C for 48 h. Fourier-transform infrared (FT-IR) spectra of the beads were recorded on an FT-IR spectrometer (model 1600, Perkin-Elmer Co.). The samples were prepared using the KBr-disk method. Wide-angle X-ray diffraction (XRD) measurement was carried out on an XRD diffractometer (D8-Advance, Bruker). The XRD patterns with Cu Kα radiation (λ = 0.15406 nm) at 40 kV and 30 mA were recorded in the region of 2θ from 8° to 50°. The magnetic properties of the composite beads were measured with a vibrating sample magnetometer (VSM, Lake Shore, 7304, USA) at 25 °C, and the hysteresis loop was obtained in a magnetic field that varied from −1.7 to +1.7 T.

2.4. Adsorption of methyl orange

The removal of organic dyes by the adsorption process in aqueous medium depends on various factors, such as contact time, initial concentration and temperature. The effect of these parameters with the affinity of the beads to methyl orange, from aqueous solution was examined. A known weight of beads (30 mg) was added to 10 mL of dye solutions in the concentrations range from 10 to 100 mg L^{-1}. The equilibrium pH of the solution was 6.7 ± 0.1 without pH adjustment. At desired time, the beads were removed from the solution by magnetic separation using a magnet. The concentration of the methyl orange in the solutions was determined with UV–vis spectrophotometer at λ_{max} = 460 nm. The removed quantity of dye by the beads was calculated by:

$$q_e = \frac{c_0 - c_e}{m} V \quad (1)$$

where c_0 (mg L^{-1}) represents the initial dye concentration, c_e (mg L^{-1}) is the equilibrium concentration of dye remaining in the solution, V (L) is the volume of the aqueous solution, and m is the weight of dry beads.

The relationship between adsorption capacity of the beads and methyl orange concentration can be expressed using the Langmuir adsorption equation and the Freundlich adsorption equation (Luo & Zhang, 2009).

$$\frac{1}{q_e} = \frac{1}{q_{max}} + \frac{1}{q_{max} b} \frac{1}{c_e} \quad (2)$$

$$\ln q_e = \frac{1}{n} \ln c_e + \ln K_F \quad (3)$$

where q_{max} is the maximum adsorption at monolayer coverage ($mg\,g^{-1}$) and b is the Langmuir adsorption equilibrium constant ($mL\,mg^{-1}$), reflecting the energy of adsorption. K_F and $1/n$ are the Freundlich characteristic constants, indicating adsorption on a surface with a finite number of identical sites. The Freundlich expression is an empirical equation based on adsorption on a heterogeneous surface.

3. Results and discussion

3.1. Formation and structure of magnetic chitin beads

The nanocomposite beads containing iron oxide were fabricated via a facile pathway. The morphologies of the CA and MCA2 are shown in Fig. 1a and b. They exhibited spherical shape with a narrow particle size distribution. The CA and MCA2 in the swollen state had average diameters of about 2 mm. However, there was lightly appreciable change in the average diameter of CA and MCA2, and only the size distribution of MCA2 was slightly broader than that of CA. This could be explained that the synthesis reaction of iron oxide occurred in the matrix of the chitin/alginate beads, and the iron oxide nanoparticles occupied only the space in the chitin/alginate. Moreover clearly, the colorless beads have transformed into reddish-brown, as a result of the formation of iron oxide component on chitin/alginate. It is worth noting that the color of the composite beads changes from light yellow to brown with increasing in the proportion of alginate in blending solution from 33 to 66%. This could be explained that alginate and iron ions could more readily cross-link compared with chitin and iron ions. Therefore, the content of iron oxide nanoparticles would be increased with the gradual increase in the proportion of alginate.

Fig. 1c and d shows SEM images of surface of the CA and MCA2, respectively. The surface of beads exhibited microporous structure. And the surface of the composite beads is denser and rougher than that of the CA, which is the contribution of inorganic nanoparticles (Liu et al., 2006).

This can be explained that the macromolecular chains of chitin and alginate could entangle each other when they were in NaOH/urea aqueous solution. It is well known that ionic cross-links will happen when alginate contacts with Ca^{2+} to form the "egg-box" structure. Moreover, multivalent counter-ions as cross-linking molecules for the formation of three dimensional alginate gels have been reported (Shi et al., 2005; Degen, Leick, & Rehage, 2009). As the chitin/alginate droplets immersed into ferrous chloride aqueous solution, Fe^{2+} could be readily cross-linking reaction with carboxyl groups on alginate chains, which entangled with chitin chains, in the chitin/alginate droplets surface. Therefore, spherical beads were observed, which indicated that ionic cross-links can also be established between the carboxyl group of alginate and iron(II). It is worth noting that when the beads with cross-linking iron(II) ions were treated with NaOH aqueous solution, rinsed with water and dried at ambient temperature, decomposition and oxidation reactions occurred (Liu et al., 2006). Thus, iron oxide nanoparticles were synthesized in situ in the matrix of the chitin/alginate to obtain the composite beads containing iron oxide.

Fig. 2a–d shows SEM images of the surface of MCAs (the MCA1, MCA2 and MCA3) and a cross-section of the MCA2. Parts a–c revealed that the iron oxide nanoparticles having spherical shape and the mean diameter of 30 nm were dispersed uniformly in the chitin/alginate matrix. The size of the iron oxide particles in the samples remained comparable with an increase in the alginate content. This could be that the chitin/alginate matrix acted as templates to limit the growth of the iron oxide nanoparticles. Part d displays obviously the inner surface of beads is more dense by filling with the iron oxide nanoparticles. The homogenous distribution of iron oxide particles in the beads revealed that chitin/alginate matrixs were used successfully as templates. As observed, the color of the nanocomposite beads turned darker, and eventually to reddish-brown due to the oxidation of Fe^{2+} into Fe^{3+}

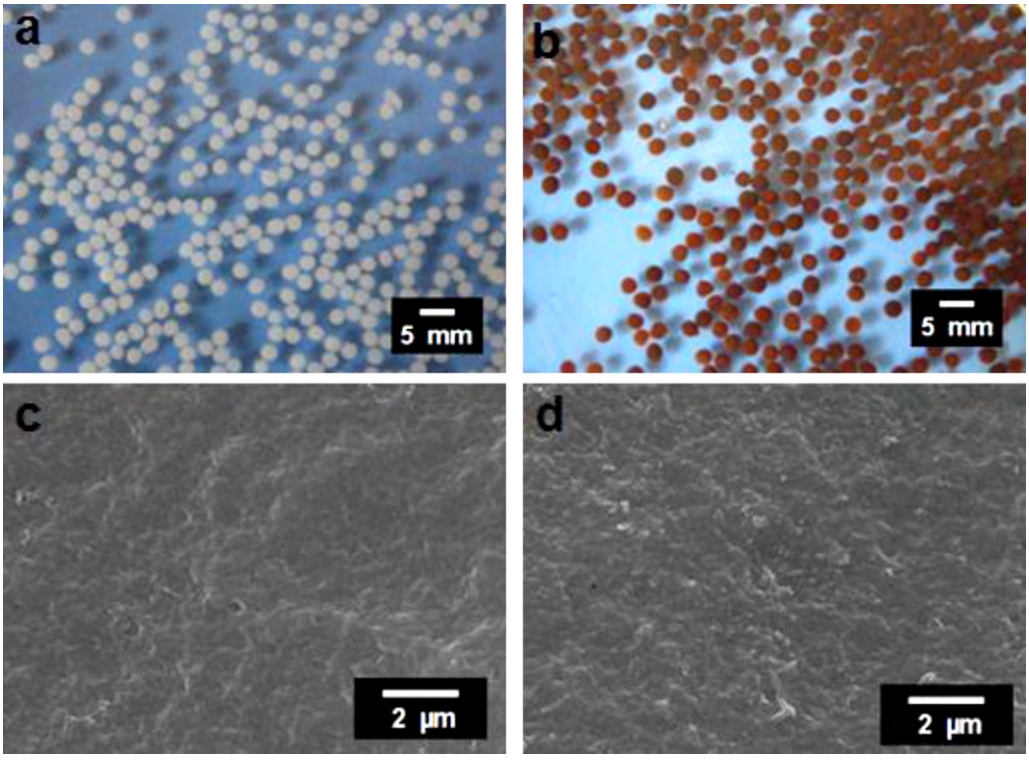

Fig. 1. The optical photographs and SEM of CA (a and c) and MCA2 (b and d), respectively.

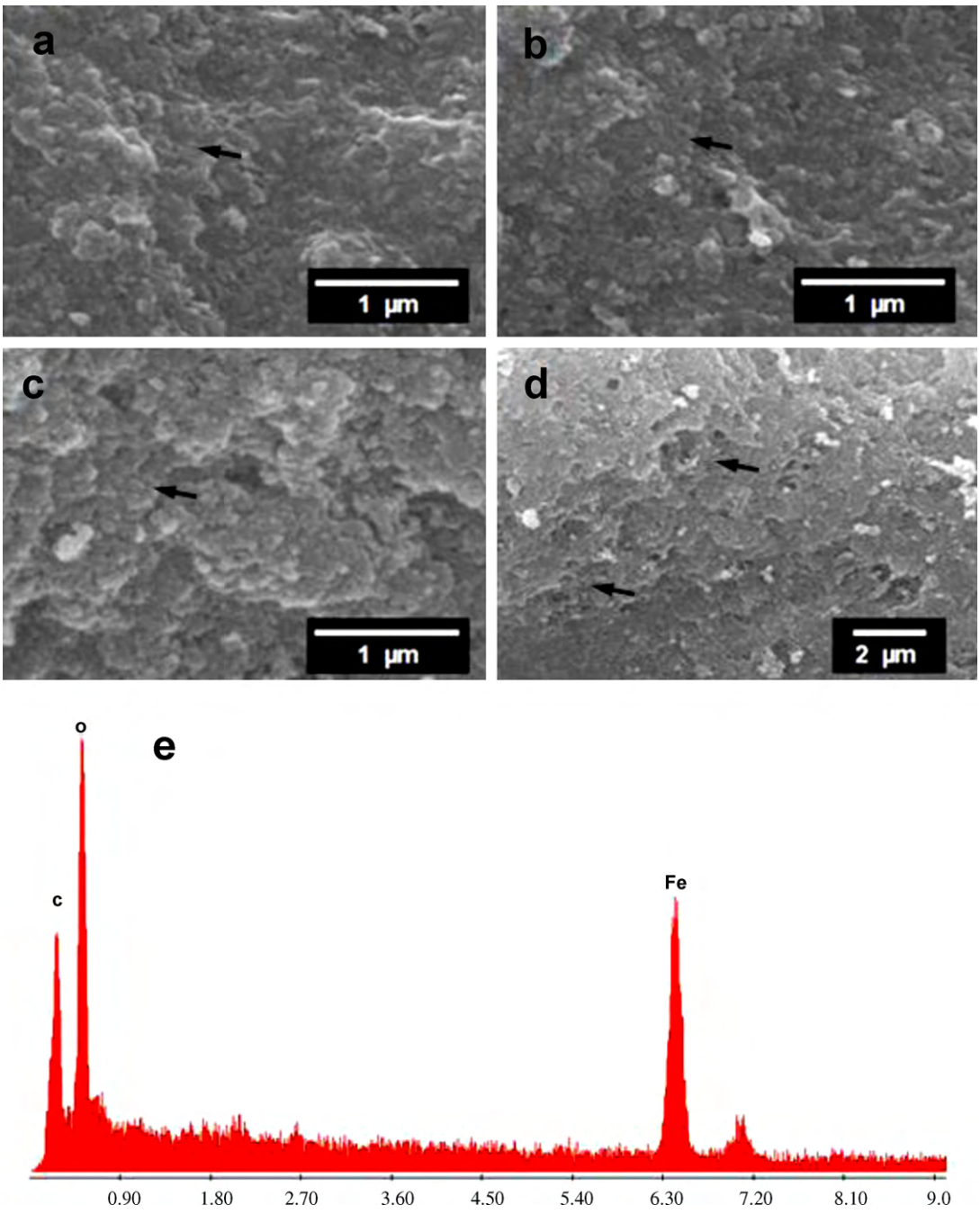

Fig. 2. SEM of the surface of MCA1 (a), MCA2 (b), MCA3 (c), SEM of the section of MCA2 (d), and EDS spectrum from SEM of MCA2 (e), respectively.

at ambient oxygen during drying and storage. Fig. 2e shows the energy-dispersive spectrum (EDS) from SEM of MCA2. There are only C, O, and Fe elements in the composite gel beads, It was further proved that the inorganic nanoparticles have been synthesized in the chitin/alginate beads.

Fig. 3a shows the FT-IR spectra of chitin, alginate, CA, and MCA2. In these spectra, a clear single peak was displayed at 1560 cm^{-1}, which was amide II band of chitin. However, it was weaker in CA that appeared at 1563 cm^{-1}, which may be caused by electrostatic interaction between carboxyl group of alginate and amino group of chitin with iron(II). Another notable change happened at 3400 cm^{-1}, which was attributed to hydroxyl stretching vibration. This band in CA was obviously broadened and shifted to lower wave number compared to alginate and chitin, indicating that intermolecular hydrogen bands may exist in the CA (Zhang, Guo, Peng, & Jin, 2004). In addition, for CA and MCA2, the peaks at 3300–3450 cm^{-1} corresponding to stretching vibrations of hydroxyl groups of polysaccharide in MCA2 moved to lower wavenumbers and became broader, indicating a strong interaction between the groups of polysaccharide and iron oxides nanoparticles through hydrogen bonding. Moreover, the new absorption peaks appeared in the range from 560 to 660 cm^{-1}, which is the characteristic absorption peaks of "Metal–O" bond (M–O), indicating the existence of the Fe–O bond (Ma, Ya, Han, & Wang, 2007). Therefore, the immobilization of nanoparticles is not only physical adsorption, but mainly chemical combination. Iron oxides are often precipitated in situ in the matrix of beads with in-beads formation of pigments for dyeing of beads (Kongdee & Bechtold, 2004),

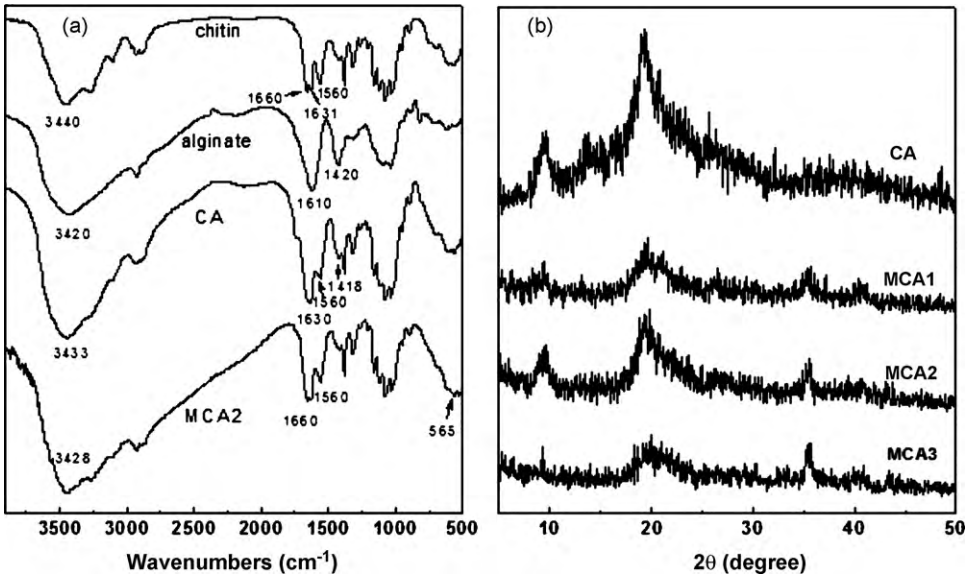

Fig. 3. FT-IR spectra (a) and the powder X-ray diffraction patterns (b).

because of the high stability of iron oxides in-beads. The stability of iron oxide nanoparticles in chitin/alginate beads is very important to the properties of the composite beads.

Fig. 3b shows the XRD patterns of the CA and nanocomposite beads. The chitin/alginate beads exhibited three peaks at $2\theta = 9.3^\circ$, 13.5°, and 19.4°, assigned to the (0 2 0), (0 2 1), and (1 1 0) planes of crystalline α-chitin, respectively (Noishiki et al., 2003). The alginate regenerated from NaOH/urea aqueous solution was quite amorphous (Zhou & Zhang, 2001). The crystallinity of chitin in the nanocomposite beads was apparently lower than that of the CA and decreased with an increase in the content of iron oxide nanoparticles. The results indicate that the crystallinity of chitin in the nanocomposites was partly destroyed because of the formation of nanoparticles. In addition, MACs displayed some distinct peaks at 2θ values of 30.7°, 35.5°, and 43.24°, assigned to the (2 2 0), (3 1 1), and (4 0 0) planes of γ-Fe_2O_3 (Liu et al., 2006). Therefore, magnetic iron oxide nanoparticles were successfully synthesized in the matrixs of the chitin/alginate by the cross-linking of Fe^{2+} ions. The mean diameters of iron oxide crystallites were also estimated using Scherrer's equation to be 26.7, 27.5, and 28.9 nm for MCA1, MCA2, and MCA3, respectively, in good agreement with the values obtained from SEM.

In view of the above results, the fabricated process of magnetic nano-gel beads via ionically cross-linked chitin/alginate could be briefly described as shown in Fig. 4.

Therefore, a direct route involving the cross-linking points of the network as reaction centers for the synthesis of the iron oxide was carried out. The chitin/alginate beads containing iron oxide were fabricated successfully by in situ synthesis of iron oxide. Moreover, to examine the bonding of iron oxide and chitin/alginate, the MCA2 was immersed in water for 60 h to analyze the iron ion contents in water. The result revealed that the amount of iron oxide nanoparticles removed from CA beads into water was found to be negligible, suggesting that there was a strong interaction between the iron oxide and CA.

3.2. Magnetic properties

The magnetic property is one of the most important characteristics of the composite beads. Fig. 5 shows the magnetization of the composite beads as a function of applied magnetic field at 298 K. The magnetization of the composite beads increases with an increase of the applied magnetic field. However, the magnetization of all composite beads is weak and shows lack of saturation, and they exhibit an extremely small hysteresis loop and low coercivity. This was a typical characteristic of some single-domain particles (Leslie-Pelecky & Rieke, 1996; Lu, Salabas, & Schuth, 2007). It is well known that magnetic particles, smaller than some critical particle diameter, can be called single domains. As the particle size continues to decrease below the single-domain value, the particles

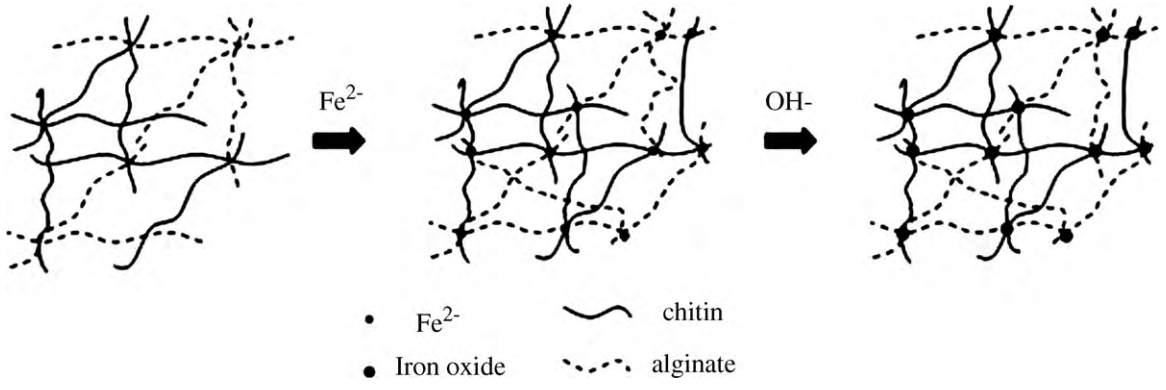

Fig. 4. Schematic illustration for the formation of the iron oxide nanocomposite beads.

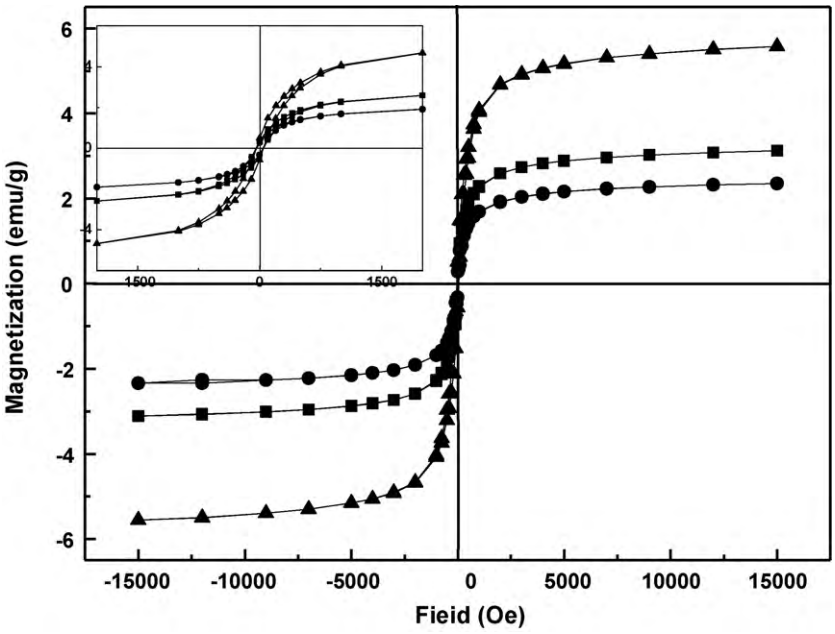

Fig. 5. The magnetic hysteresis loops of the composite beads MCA1 (●), MCA2 (■) and MCA3 (▲) at 298 K. Insert: a magnified view of the −2000 to 2000 Oe regions.

exhibit superparamagnetic properties. On the one hand, a single-domain particle is uniformly magnetized with all the spins aligned in the same direction. The magnetization will be reversed by spin rotation since there are no domain walls to move. On the other hand, the shape anisotropy is another source for the coercivity in a system of small particles. The departure from sphericity for single-domain particles is significant and has an influence on the coercivity. Therefore, There was some low coercivity observed in nanocomposite beads (as shown in Fig. 5 insert). And the characteristic of superparamagnetic iron oxide nanoparticles in MCA2 was better than the others. With an increase of the iron content, the coercivity of the particles became more obvious. Therefore, the MCA2 sample was used mainly for the investigations on the adsorption behaviors of organic dyes. The saturation magnetization of MCA1, MCA2 and MCA3 obtained from the hysteresis loop was 2.35, 3.12, and 5.58 emu/g, respectively, depending on the iron oxide content. Moreover, it is interesting that these magnetic composite beads (MCAs) with iron oxide nanoparticles could align in the magnetic field within a short time, which revealed that the MCAs could move directionally by introducing a magnetic field. Therefore, the MCAs possessed a sensitive magnetic response, which is important for their application. Hence, we provide here a facile and green method to fabricate magnetic nanocomposites beads with high nanophase contents and metal oxide nanoparticles.

3.3. Adsorption behaviors of methyl orange

The adsorption experiments to evaluate the contact time effect on MO removal by beads were carried out ranging from 0 to 6 h, at the 298 K. The results are presented in Fig. 6a. It is obvious that the amount of adsorbed methyl orange on the beads increased with an increase in time, moreover, the adsorption amounts of MO increased rapidly in the initial 3 h and almost unchanged after 5 h, indicating an equilibrium state. Therefore, methyl orange adsorption loading can be controlled by changing the time. Furthermore, the magnetic chitin beads possessed higher MO adsorption capacity than CA. This could be explained that more specific surface area was obtained for composite beads because of the microporous structure and formation of iron oxide nanoparticles, which can be more easily adsorbed dye molecules. Therefore, the iron oxide nanoparticles of composite beads play an important role in the improvement of both the adsorption capacity and the adsorption rate.

In addition, the relationship between the adsorption capacity and the original MO concentration was examined. The adsorption

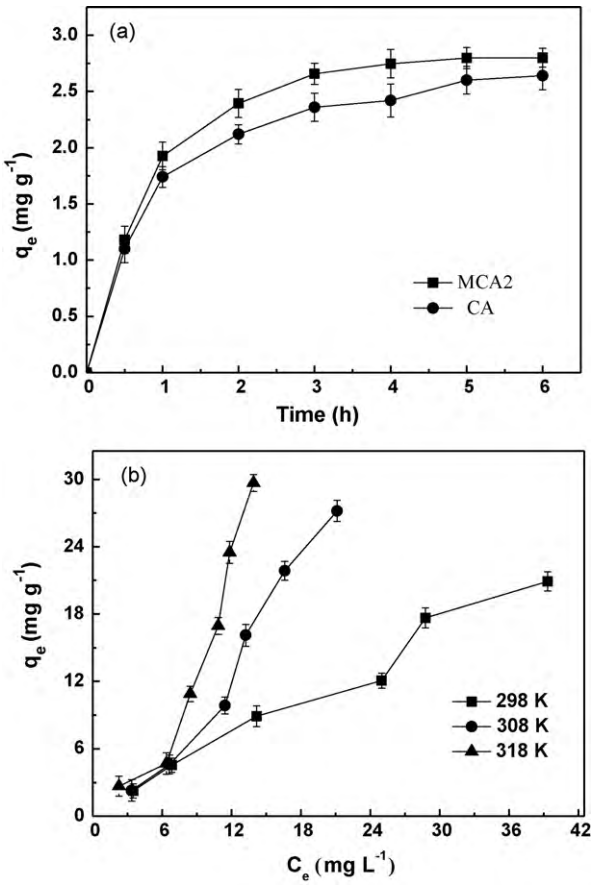

Fig. 6. Time dependence of MO adsorption loading of MCA2 (■) and CA (●) (c_0 = 12.5 mg L^{-1}, T = 298 K) (a) and adsorption isotherms of MO adsorbed onto MCA2 in aqueous solution at 298, 308, and 318 K (b), respectively.

Table 1
Langmuir, Freundlich isotherm constants and Gibbs free energy, entropy changes for adsorption of MO by MCA2.

T (K)	Langmuir model			Freundlich model			ΔG (kJ mol^{-1})	ΔH (kJ mol^{-1})	ΔS (J mol^{-1} K^{-1})
	q_m (mg g^{-1})	b (L mg^{-1})	R	$1/n$	K_F (mg g^{-1})	R			
298	107.5	0.4261	0.9986	0.9087	97.4	0.9943	−10.52	4.545	64.92
308	116.3	0.3652	0.9974	0.8713	104.3	0.9903	−12.87		
318	128.5	0.3285	0.9746	0.8350	113.8	0.9432	−23.33		

capacity increases with an increase in the initial concentration, which indicates that the initial concentration has significant effect on the adsorption of MO. And the percentage of MO removal decreased with increasing initial MO concentration from 82.1% for 10 mg L^{-1} to 67.3% for 100 mg L^{-1}. It could be explained by the fact that the amount of substance for MO increases as the high initial concentration, however, the total numbers of available adsorption sites are fixed for a given adsorbent dose, which adsorbs almost the same amount of dye. Thus, the high initial concentration is not conducive to the improvement of the percentage removal of dye. Similar results have been reported by Ni, Xia, Wang, Xing, and Pan (2007).

The relationship between the adsorption capacity and the temperature was examined, and was analyzed by both the Langmuir and Freundlich isotherms. Fig. 6b shows the adsorption isotherms of MO on MCA2 in aqueous solution at 298, 308, and 318 K, respectively. It is clear that the adsorption capacity increases with the increase in the temperature. This may be explained that a higher temperature could promote the process of adsorption. Indeed, high temperature could increase the mobility of dye molecules, which leads to the faster absorption rate. However, it will not affect the absorption capacity. Instead, high temperature can cause the swelling of beads, which may lead to an increase of surface area and consequently increase the absorption capacity. The calculated data from Langmuir and Freundlich isothermal adsorption parameters for the MO adsorption are summarized in Table 1. It is seen that the Langmuir isotherm is more suitable to characterize the adsorption due to the higher correlation coefficient R than 0.998. Therefore, the Langmuir model was used to describe the MO adsorption. It indicated that the MO was adsorbed on the beads as a monolayer adsorption. The q_{max} value of MCA2 indicated the excellent adsorption ability of the composite beads.

Adsorption enthalpy (ΔH), adsorption free energy (ΔG), and adsorption entropy (ΔS) can be calculated as (Ni et al., 2007; Huang, Huang, Liu, Wang, & Yan, 2008):

$$\ln c_e = \frac{\Delta H}{RT} + \ln K \quad (4)$$

$$\Delta G = -RT \ln k \quad (5)$$

$$\Delta S = \frac{\Delta H - \Delta G}{T} \quad (6)$$

where R is the ideal gas constant (8.314 kJ mol^{-1} K^{-1}), T is the absolute temperature (K), K is a constant, and k is the Langmuir constant ($k = bq_m$). From Eq. (4), ΔH can be figure out from the isosters, plot of $\ln c_e$ vs $1/T$ (not shown). The correlated isosters are straight lines and then ΔH can be calculated from the slope of the straight line. The ΔH, ΔG, and ΔS of MO adsorbed onto MCA2 are listed in Table 1. The positive ΔH indicates that the adsorption is endothermic, therefore, the high temperature is more conducive to adsorption process, which consistents with the results of the adsorption isotherms. The negative ΔG implies the spontaneous adsorption process, and it is independent of the adsorption capacity. The positive ΔS suggests the increased randomness at the solid/solution interface during the adsorption of MO on MCA2.

4. Conclusions

Novel magnetic chitin/alginate gel beads were synthesized successfully in situ using the ionically cross-linked method. This is a new and simple method for the preparation of magnetic chitin-based gel beads, which are safe, biocompatible and biodegradable. The iron oxide nanoparticles were dispersed uniformly in the chitin/alginate matrix, as a result of a strong interaction between iron oxide and the polymers. The nanocomposite beads exhibited sensitive magnetic-inducted delivery and superparamagnetic properties. Iron oxide nanoparticles play an important role in both the creation of the magnetic-induced transference and the improvement of the adsorption capacity. Moreover, methyl orange as models of organic dyes was adsorbed effectively by the composite beads, and could be described well by Langmuir isotherms. The magnetic properties of the beads allow their separation from the effluent by applying amagnetic field, leading to the development of a clean and safe process for water pollution remediation. This work provides a promising technique to fabricate magnetic chitin-based nanocomposite materials, which has potential application on the removal of hazardous materials.

Acknowledgements

We thank Dr. Wei Li (School of Resource and Environmental Science, Wuhan University) and Dr. Yongbo Song (Department of Chemistry, Wuhan University) for enthusiastic support and helpful discussions.

References

Acosta, N., Aranaz, I., Peniche, C., & Heras, A. (2003). Tramadol release from a delivery system based on alginate-chitosan microcapsules. *Macromolecular Bioscience*, *3*, 546–551.
Akkaya, G., Uzun, I., & Guzel, F. (2009). Adsorption of some highly toxic dyestuffs from aqueous solution by chitin and its synthesized derivatives. *Desalination*, *249*, 1115–1123.
Arai, T., Sato, T., Kanoh, H., Kaneko, K., Oguma, K., & Yanagisawa, A. (2008). Organic-inorganic hybrid polymer-encapsulated magnetic nanobead catalysts. *Chemistry: A European Journal*, *14*, 882–885.
Degen, P., Leick, S., & Rehage, H. (2009). Mechanical stability of ionotropic alginate beads. *International Journal of Research in Physical Chemistry & Chemical Physics*, *223*, 1079–1090.
Ge, Y. Q., Zhang, Y., He, S. Y., Nie, F., Teng, G. J., & Gu, N. (2009). Fluorescence modified chitosan-coated magnetic nanoparticles for high-efficient cellular imaging. *Nanoscale Research Letters*, *4*, 287–295.
Gruttner, C., Rudershausen, S., & Teller, J. (2001). Improved properties of magnetic particles by combination of different polymer materials as particle matrix. *Journal of Magnetism and Magnetic Materials*, *225*, 1–7.
Hu, X. W., Du, Y. M., Tang, Y. F., Wang, Q., Feng, T., Yang, J. H., et al. (2007). Solubility and property of chitin in NaOH/urea aqueous solution. *Carbohydrate Polymers*, *70*, 451–458.
Hu, X., Du, Y., Li, G., & Wang, Q. (2008). Preparation and properties of chitin/sodium alginate blend fiber. *Journal of Wuhan University (Natural Science Edition)*, *54*, 697–702.
Huang, J. H., Huang, K. L., Liu, S. Q., Wang, A. T., & Yan, C. (2008). Adsorption of Rhodamine B and methyl orange on a hypercrosslinked polymeric adsorbent in aqueous solution. *Colloids and Surfaces A: Physicochemical and Engineering Aspects*, *330*, 55–61.
Jarzyna, P. A., Skajaa, T., Gianella, A., Cormode, D. P., Samber, D. D., Dickson, S. D., et al. (2009). Iron oxide core oil-in-water emulsions as a multifunctional nanoparticle platform for tumor targeting and imaging. *Biomaterials*, *30*, 6947–6954.
Kongdee, A., & Bechtold, T. (2004). In-fibre formation of $Fe(OH)_3$ – A new approach to pigment coloration of cellulose fibres. *Dyes and Pigments*, *60*, 137–142.

Kroll, E., & Winnik, F. M. (1996). In situ preparation of nanocrystalline Fe_2O_3 in iron (II) cross-linked alginate gels. *Chemical Materials*, *8*, 1594–1596.
Leslie-Pelecky, D. L., & Rieke, R. D. (1996). Magnetic properties of nanostructured materials. *Chemistry of Materials*, *8*, 1770–1783.
Li, G., Du, Y., Tao, Y., Liu, Y., Li, S., Hu, X., et al. (2010). Dilute solution properties of four natural chitin in NaOH/urea aqueous system. *Carbohydrate Polymers*, *80*, 970–976.
Liu, W. T. (2006). Nanoparticles and their biological and environmental applications. *Journal of Bioscience and Bioengineering*, *102*, 1–7.
Liu, S. L., Zhou, J. P., Zhang, L. N., Guan, J. G., & Wang, J. B. (2006). Synthesis and alignment of iron oxide nanoparticles in a regenerated cellulose film. *Macromolecular Rapid Communications*, *27*, 2084–2089.
Liu, S., Zhang, L., Zhou, J., & Wu, R. (2008). Structure and properties of cellulose/Fe_2O_3 nanocomposite fibers spun via aneffective pathway. *Journal of Physical Chemistry C*, *112*, 4538–4544.
Lu, A. H., Salabas, E. L., & Schuth, F. (2007). Magnetic nanoparticles: Synthesis, protection, functionalization, and application. *Angewandte Chemie International Edition*, *46*, 1222–1244.
Luo, X., & Zhang, L. (2009). Hight effective adsorption of organic dyes on magnetic cellulose beads entrapping actived carbon. *Journal of Hazardous Materials*, *171*, 340–347.
Luo, X., Liu, S., Zhou, J., & Zhang, L. (2009). In situ synthesis of Fe_3O_4/cellulose microspere with magnetic-induced protein delivery. *Journal of Materials Chemisty*, *19*, 3538–3545.
Ma, H. L., Qi, X. T., Maitani, Y., & Nagai, T. (2007). Preparation and characterization of superparamagnetic iron oxide nanoparticles stabilized by alginate. *International Journal of Pharmaceutics*, *333*, 177–186.
Ma, W., Ya, F. Q., Han, M., & Wang, R. (2007). Characteristics of equilibrium, kinetics studies for adsorption of fluoride on magnetic-chitosan particle. *Journal of Hazardous Materials*, *143*, 296–302.
Miretzky, P., & Cirelli, A. F. (2009). Hg(II) removal from water by chitosan and chitosan derivatives: A review. *Journal of Hazardous Materials*, *167*, 10–23.
Mironov, V. L., & Ermolaeva, O. L. (2009). Optimization of a data storage system based on the array of ferromagnetic particles and magnetic force microscope. *Journal of Surface Investigation: X-Ray Synchrotron and Neutron Techniques*, *3*, 840–845.
Morais, P. C., Santos, J. G., Silveira, L. B., & Oliveira, A. C. (2007). The effect of the particle concentration in biocompatible magnetic fluids: A dynamical susceptibility investigation. *Journal of Alloys and Compounds*, *434*, 608–610.
Ni, Z. M., Xia, S. J., Wang, L. G., Xing, F. F., & Pan, G. X. (2007). Treatment of methyl orange by calcined layered double hydroxides in aqueous solution: Adsorption property and kinetic studies. *Journal of Colloid and Interface Science*, *316*, 284–291.
Noishiki, Y., Takami, H., Nishiyama, Y., Wada, M., Kada, S., & Kuga, S. (2003). Alkali-induced conversion of beta-chitin to alpha-chitin. *Biomacromolecules*, *4*, 896–899.
Oliveira, F. C. C., Rossi, L. M., Jardim, R. F., & Rubim, J. C. (2009). Magnetic fluids based on gamma-Fe_2O_3 and $CoFe_2O_4$ nanoparticles dispersed in ionic liquids. *Journal of Physical Chemistry C*, *113*, 8566–8572.
Rinaudo, M. (2006). Chitin and chitosan: Properties and applications. *Progress in Polymer Science*, *31*, 603–632.
Rocher, V., Siauque, J. M., Cabuil, V., & Bee, A. (2008). Removal of organic dyes by magnetic alginate beads. *Water Research*, *42*, 1290–1298.
Shi, X. W., Du, Y. M., Sun, L. P., Yang, J. H., Wang, X. H., & Su, X. L. (2005). Ionically crosslinked alginate/carboxymethyl chitin beads for oral delivery of protein drugs. *Macromolecular Bioscience*, *5*, 881–889.
Soenen, S. J. H., Hodenius, M., & De Cuyper, M. (2009). Magnetoliposomes: Versatile innovative nanocolloids for use in biotechnology and biomedicine. *Nanomedicine*, *4*, 177–191.
Suckow, M. A., Jarvinen, L. Z., HogenEsch, H., Park, K., & Bowersock, T. L. (2002). Immunization of rabbits against a bacterial pathogen with an alginate microparticle vaccine. *Journal of Controlled Release*, *85*, 227–235.
Sun, L., Chen, L. G., Sun, X., Du, X. B., Yue, Y. S., He, D. Q., et al. (2009). Analysis of sulfonamides in environmental water samples based on magnetic mixed hemimicelles solid-phase extraction coupled with HPLC-UV detection. *Chemosphere*, *77*, 1306–1312.
Tansil, N. C., Ramanujan, R. V., & Li, H. F. (2003). Chemical synthesis of FeCo nanocrystals for massive data storage applications. *Transactions of the Indian Institute of Metals*, *56*, 509–512.
Tartaj, P., Morales, M. D., Veintemillas-Verdaguer, S., Gonzalez-Carreno, T., & Serna, C. J. (2003). The preparation of magnetic nanoparticles for applications in biomedicine. *Journal of Physics D: Applied Physics*, *36*, R182–R197.
Wan, J., Cai, W., Meng, X., & Liu, E. (2007). Monodisperse water-soluble magnetite nanoparticles prepared by polyol process for high-performance magnetic resonance imaging. *Chemical Communications*, 5004–5006.
Xu, J., Mccarthy, S. P., Gross, R. A., & Kaplan, D. L. (1996). Chitosan film acylation and effects on biodegradability. *Macromolecules*, *29*, 3436–3440.
Zhang, L., Guo, J., Peng, X. H., & Jin, Y. (2004). Preparation and release behavior of carboxymethylated chitosan/alginate microspheres encapsulating bovine serum albumin. *Journal of Applied Polymer Science*, *92*, 878–882.
Zheng, H., Zhou, J. P., Du, Y. M., & Zhang, L. N. (2002). Cellulose/chitin films blended in NaOH/urea aqueous solution. *Journal of Applied Polymer Science*, *86*, 1679–1683.
Zheng, Y., Duanmu, C., & Gao, Y. (2006). A magnetic biomimetic nanocatalyst for cleaving phosphoester and carboxylic ester bonds under mild conditions. *Organic Letters*, *8*, 3215–3217.
Zhou, J., & Zhang, L. (2001). Structure and properties of blend membranes prepared from cellulose and alginate in NaOH/urea aqueous solution. *Journal of Polymer Science: Part B: Polymer Physics*, *39*, 451–458.
Zhou, D., Zhang, L., & Guo, S. L. (2005). Mechanisms of lead biosorption on cellulose/chitin beads. *Water Research*, *39*, 3755–3762.